York, C. B. and Almeida, S. F. M. d. (2017) Effect of Design Heuristics on the Compression and Shear Buckling Performance of Infinitely Long Plates With Bending-Twisting Coupling. 21st International Conference on Composite Materials, Xi'an, China, 20-25 Aug 2017.

http://eprints.gla.ac.uk/141514/

Deposited on: 23 May 2017

Enlighten – Research publications by members of the University of Glasgow
http://eprints.gla.ac.uk

# EFFECT OF DESIGN HEURISTICS ON THE COMPRESSION AND SHEAR BUCKLING PERFORMANCE OF INFINITELY LONG PLATES WITH BENDING-TWISTING COUPLING.

Christopher Bronn York[1] and Sérgio Frascino Müller de Almeida[2]

[1] Aerospace Sciences, School of Engineering, University of Glasgow, University Avenue, G12 8QQ, Glasgow, Scotland, Christopher.York@Glasgow.ac.uk, http://www.gla.ac.uk/schools/engineering/staff/christopheryork/

[2] Department of Mechatronics and Mechanical Systems Engineering, University of São Paulo, Av. Professor Mello Moraes, 2231, São Paulo, SP, 05508-030, Brazil, sergio.frascino@gmail.com.

**Keywords:** Composite plates, Bending-Twisting Coupling, Buckling, Ply Percentages, Ply Contiguity.

## ABSTRACT

This article investigates the effect of design heuristics, including ply percentages and ply contiguity constraints, on the compression and shear buckling performance of *Bending-Twisting* coupled infinitely long laminated plates with simply supported edges. The buckling solutions are presented as contour maps, representing non-dimensional buckling factors, which are superimposed on the lamination parameter design spaces for laminates with standard ply orientations. The applicability of the results extends beyond the current certification envelope, comprising symmetric laminate configurations. Indeed, the contour maps are applicable to two recently developed databases containing non-symmetric and symmetric laminates with either *Bending-Twisting* or *Extension-Shearing Bending-Twisting* coupling. The contour maps provide insights into buckling performance improvements that are non-intuitive and facilitate comparison between hypothetical and practical designs. The databases are illustrated through point clouds of lamination parameter coordinates, which demonstrate the effect of applying design heuristics.

## 1 INTRODUCTION

Recent research has led to laminate design databases containing *Extension-Shearing* [1] and/or *Bending-Twisting* coupling [2]. The results have demonstrated that the design spaces contain predominantly non-symmetric stacking sequences. All are immune to thermal warping distortions by virtue of the fact that their coupling stiffness properties are null (**B** = **0**); as would be expected from symmetric laminate configurations. Heuristic design rules [3] are applied to these databases to assess the effect on buckling performance on a reduced design space, representing practical rather than hypothetical designs.

The data are presented as lamination parameter [4] point clouds, where each point represents an individual laminate design. The use of standard ply orientations, i.e. 0°, 90° and ±45° plies, results in a feasible design space defined by a regular tetrahedron. The application of the 10% rule, corresponding to a minimum of 10% plies in each of the standard ply orientations, is illustrated in Fig. 1 for extensional stiffness. The bounds of the 10% rule form a triangular plane within the feasible region of the design space when the extensional stiffness is uncoupled, i.e. for *Bending-Twisting* coupled only designs, and forms a reduced tetrahedron when *Extension-Shearing* (and *Bending-Twisting*) coupled is present.

By contrast, the lamination parameter point clouds for bending stiffness are illustrated in Fig. 2. Here, the effect of the 10% rule appears to have limited impact on the extent of the point clouds, in view of the proximity to the bounds of the feasible region, which is significant given that these regions correspond to upper-bound buckling load solutions.

A set of high fidelity orthographic projections, given in Fig. 3, help to provide further detail of the 10% rule, and are described later in the context of the impact of this in-plane material constraint on the out-of-plane material properties, with specific reference to *Bending-Twisting* coupling.

New insights into compression and shear buckling strength are provided via buckling factor contour maps, which are superimposed onto the lamination parameter design spaces. Contour mapping is applied to cross-sections through the design space, to allow detailed interrogation of the effects of *Bending-Twisting* coupling on buckling strength. The mapping is also applied to external surfaces of the feasible domain of lamination parameters, since these surfaces represent the bounds on buckling strength. The results are applicable to infinitely long plates, which represent useful lower-bound solutions for preliminary design optimisation.

## 2 BUCKLING OF INFINITELY LONG PLATES

Bounds on the buckling performance of (infinitely) long, simply supported, 'symmetric' *Bending-Twisting* coupled laminates have been extensively investigated under both compression [5] and/or shear [6,7]. Hence, in view of the significant number of non-symmetric and other forms of sub-sequence symmetry identified elsewhere [1, 2], which result in a vast increase in the possible design space for *Bending-Twisting* coupled laminate designs, the possibility of additional gains in buckling performance, above symmetric laminates, can now be explored.

Infinitely long compression loaded plates with simply supported edges provide a convenient lower-bound solution, and are useful for preliminary design. A closed form solution, necessary to handle the vast number of designs, can also be used to assess the buckling strength exactly:

$$N_{x,\infty} = \pi^2 \left[ D_{11} \left[ \frac{1}{\lambda} \right]^2 + 2\left(D_{12} + 2D_{66}\right) \frac{1}{b^2} + D_{22} \left[ \frac{1}{b^4} \right] \lambda^2 \right] \tag{1}$$

For *Bending-Twisting* coupled laminates, approximate closed form solutions must be adopted [8, 9], or developed. Noting however that there are no closed form solutions for shear loaded plates, the following section develops new closed form solutions applicable to both compression and shear buckling.

### 2.1 Closed form solution for Compression Buckling

For orthotropic laminates, the following buckling equation, representing a 2 dimensional, 4$^{th}$ order polynomial can be solved against the exact closed form buckling solution from equally spaced points across the lamination parameter design space:

$$\begin{aligned} k_\infty = {} & c_1 + c_2\xi_\Delta^D + c_3\xi_R^D + c_4\left(\xi_\Delta^D\right)^2 + c_5\left(\xi_R^D\right)^2 + c_6\xi_\Delta^D\xi_R^D + c_7\left(\xi_\Delta^D\right)^3 + c_8\left(\xi_R^D\right)^3 + c_9\xi_\Delta^D\left(\xi_R^D\right)^2 \\ & + c_{10}\left(\xi_\Delta^D\right)^2\xi_R^D + c_{11}\left(\xi_\Delta^D\right)^4 + c_{12}\left(\xi_R^D\right)^4 + c_{13}\xi_\Delta^D\left(\xi_R^D\right)^3 + c_{14}\left(\xi_\Delta^D\right)^2\left(\xi_R^D\right)^2 + c_{15}\left(\xi_\Delta^D\right)^3\xi_\nu^D \end{aligned} \tag{2}$$

where in this case, $k_\infty = k_{x,\infty}$ and is defined by:

$$k_{x,\infty} = \frac{N_{x,\infty} b^2}{\pi^2 D_{Iso}} \tag{3}$$

The lamination parameters are related to the bending stiffness matrix [**D**] by:

$$\left[\mathbf{D}\right] = \frac{H^3}{12} \begin{bmatrix} U_E + \xi_\Delta^D U_\Delta + \xi_R^D U_R & U_E - 2U_G - \xi_R^D U_R & \xi_{\Delta c}^D U_\Delta / 2 + \xi_{Rc}^D U_R \\ U_E - 2U_G - \xi_R^D U_R & U_E - \xi_\Delta^D U_\Delta + \xi_R^D U_R & \xi_{\Delta c}^D U_\Delta / 2 - \xi_{Rc}^D U_R \\ \xi_{\Delta c}^D U_\Delta / 2 + \xi_{Rc}^D U_R & \xi_{\Delta c}^D U_\Delta / 2 - \xi_{Rc}^D U_R & U_G - \xi_R^D U_R \end{bmatrix} \tag{4}$$

Noting that $\xi_{Rc}^D = 0$ for standard ply orientations.

The laminate invariants are defined in terms of the reduced stiffnesses:

$$
\begin{aligned}
U_E &= \left(3Q_{11} + 3Q_{22} + 2Q_{12} + 4Q_{66}\right)/8 \\
U_G &= \left(Q_{11} + Q_{22} - 2Q_{12} + 4Q_{66}\right)/8 \\
U_\Delta &= \left(Q_{11} - Q_{22}\right)/2 \\
U_R &= \left(Q_{11} + Q_{22} - 2Q_{12} - 4Q_{66}\right)/8
\end{aligned} \tag{5}
$$

$$D_{iso} = U_E H^3/12 \tag{6}$$

Exact buckling factor results are established at 15 sample points corresponding to the grid point intersections, formed by the equilateral triangles, illustrated on the cross-section in Fig. 4(a). These results give rise to the coefficients $c_1 - c_{15}$ in Eq. (2), leading to the following closed form solution, which is applicable to all fully uncoupled laminates [10]:

$$
\begin{aligned}
k_{x,\infty} = {} & 4.000 - 1.049\xi_R^D - 1.217\left(\xi_\Delta^D\right)^2 + 0.340\xi_R^D\left(\xi_\Delta^D\right)^2 \\
& - 0.360\left(\xi_\Delta^D\right)^4 - 0.034\left(\xi_R^D\right)^2\left(\xi_\Delta^D\right)^2
\end{aligned} \tag{7}
$$

Equation (7) is used to develop the isolines of constant buckling factor, $k_{x,\infty}$, which are illustrated on Fig. 4(b). The top corners of the triangular region of Fig. 4(b), representing laminates with 90° or 0° degree plies only, have buckling factor $k_{x,\infty}$ = 1.68 (with buckling half-waves $b/\lambda$ = 1.94 = $(D_{22}/D_{11})^{¼}$ and $\lambda/b$ = 1.94, respectively), whereas the bottom corner, representing laminates with ±45° plies only, has buckling factor $k_{x,\infty}$ = 5.05 (with buckling half-wave $\lambda = b$). The centre of the contour map, represents the fully isotropic laminate, and for which all lamination parameters are zero, gives the classical buckling factor result, $k_{x,\infty}$ = 4.00.

The three dimensional representation of the feasible design space in Fig. 4(a) indicates the positions through which other cross-sections are taken in order to maintain constant magnitude of *Bending-Twisting* coupling.

For *Bending-Twisting* coupled laminates, ($\xi_{\Delta c}^D \neq 0$) an exact infinite strip analysis [11] has been adopted to generate buckling factors at the same relative grid point locations, as illustrated on Fig. 4(a), for each discrete cross-section throughout the lamination parameter design space. This analysis was also used as a validation process for the compression buckling results. Coefficients for other cross-sections throughout the lamination parameter design space, $0 \leq \xi_{\Delta c}^D \leq 0.9$, are given in Table 1.

Note:

- When $\xi_{\Delta c}^D = \pm 1.0$, the design space degenerates to a single point with $k_{x,\infty}$ = 2.19.
- Lamination parameter bounds are $-1.0 \leq \xi_{\Delta c}^D \leq 1.0$. Negative $\xi_{\Delta c}^D$ are to positive $\xi_{\Delta c}^D$.

The buckling strength relationship at any cross-section is determined by substituting the appropriate coefficients of Table 1 into Eq. (2). Note that the number of significant figures in the coefficients of Table 1 have been reduced, but are sufficient to maintain a buckling factor accurate to 2 decimal places.

### 2.2 Closed form solution for Shear Buckling

For shear bucking, the same procedure is adopted as for compression buckling, using the exact infinite strip analysis [11] to generate buckling factors at the same relative grid point locations, as illustrated on Fig. 4(a).

For the orthotropic laminate, the closed form solution for positive and negative shear loading is identical and is obtained by substituting the calculated coefficients into Eq. (2).

$$
\begin{aligned}
k_{xy,\infty} = {} & 5.336 - 2.914\xi_{\Delta}^{D} - 0.518\xi_{R}^{D} - 1.303\left(\xi_{\Delta}^{D}\right)^{2} - 0.213\left(\xi_{R}^{D}\right)^{2} + 1.048\xi_{\Delta}^{D}\xi_{R}^{D} \\
& - 0.236\left(\xi_{\Delta}^{D}\right)^{3} + 0.031\left(\xi_{R}^{D}\right)^{3} - 0.197\xi_{\Delta}^{D}\left(\xi_{R}^{D}\right)^{2} + 0.405\left(\xi_{\Delta}^{D}\right)^{2}\xi_{R}^{D} - 0.443\left(\xi_{\Delta}^{D}\right)^{4} \\
& - 0.001\left(\xi_{R}^{D}\right)^{4} + 0.022\xi_{\Delta}^{D}\left(\xi_{R}^{D}\right)^{3} - 0.185\left(\xi_{\Delta}^{D}\right)^{2}\left(\xi_{R}^{D}\right)^{2} + 0.472\left(\xi_{\Delta}^{D}\right)^{3}\xi_{\nu}^{D}
\end{aligned}
\tag{8}
$$

where in this case, $k_{\infty} = k_{xy,\infty}$ and is defined by:

$$
k_{xy,\infty} = \frac{N_{xy,\infty} b^{2}}{\pi^{2} D_{Iso}} \tag{9}
$$

and gives the classical shear buckling factor result, $k_{xy,\infty} = 5.34$ [12], for the isotropic design; when all lamination parameters are set to zero. The resulting contour map is illustrated in Fig. 4(c), illustrating isolines of constant buckling load factor across the lamination parameter design space. Positive shear direction is defined together with positive fibre angle direction in Fig. 4(a). The top corners of the triangular region of Fig. 4(c), representing laminates with 90° and 0° degree plies only, have shear buckling factors $k_{xy,\infty} = 4.91$ and 1.31, respectively, whereas the bottom corner, representing laminates with ±45° plies only, has buckling factor $k_{xy,\infty} = 5.61$.

For *Bending-Twisting* coupled laminates, $\xi_{\Delta c}^{D} \neq 0$, coefficients for other cross-sections within the lamination parameter designs space, $0 \leq \xi_{\Delta c}^{D} \leq 0.9$, have been calculated for positive and negative shear respectively, but tables containing these coefficients are not presented due to space limitations.
Note:

- When $\xi_{\Delta c}^{D} = 1.0$, the design space degenerates to a point with minimum and maximum $k_{xy,\infty} = 1.38$ and 8.84, for positive and negative shear, respectively.
- Lamination parameter bounds are $-1.0 \leq \xi_{\Delta c}^{D} \leq 1.0$. Negative $\xi_{\Delta c}^{D}$ are synonymous with a reversal in the shear load direction, hence only positive $\xi_{\Delta c}^{D}$ are given.

Ignoring the effects of *Bending-Twisting* coupling continues to broadly justified on the basis that the effects dissipate for laminates with a large number of plies. However, buckling strength is strongly influenced by such coupling in thin laminates; shear buckling strength may be overestimated (unsafe) or underestimated (over-designed) if the effects of *Bending-Twisting* coupling are ignored. This can be appreciated by the fact that shear loading and *Bending-Twisting* coupling ($\xi_{\Delta c}^{D} \neq 0$) both give rise to skewed nodal lines in the buckling mode shapes. Hence, the presence of *Bending-Twisting* coupling may augment or counter the effect of shear load, depending on whether the resulting diagonal tension is perpendicular or parallel to the dominant angle-ply direction.

### 2.3 Contour mapping

The closed form solution of Eq. (2), together with the associated coefficients, are used to develop the selection of contours maps that follow.

Figure 5 represents a series of compression buckling factor contour maps, corresponding to gradually increasing magnitude in *Bending-Twisting* coupling. The symmetric contours of the fully uncoupled designs, of Fig. 4(b), now give way to *increasing* asymmetry in the contour pattern.

This contour mapping is applied to cross-sections through the design space, to allow detailed interrogation of the effects of *Bending-Twisting* coupling on buckling strength.

The mapping is also applied to external surfaces of the feasible domain of lamination parameters in Figs 8 and 9, since these surfaces represent the bounds on buckling factor. These surface contours reveal local optima in locations that are non-intuitive, i.e. the optimum shear buckling factor $k_{xy,\infty} = 9.06$ @ ($\xi_{\Delta}^{D}, \xi_{R}^{D}, \xi_{\Delta c}^{D}$) = (-0.18, -0.64, -0.82), which exceeds $k_{xy,\infty} = 8.84$ at $\xi_{\Delta c}^{D} = 1.0$.

## 3 Design space reduction – Heuristic constraints

Figures 10 and 11 provided high fidelity orthographic projections of design space for laminates with *Extension-Shearing Bending-Twisting* coupling. Each point within the 3-dimensional design space represents a physical design, for which a stacking sequence is known. These results represent the available solutions after applying the 10% design rule and can be compared to the full design space, presented elsewhere [2]. The key observation is that the impact on the design space for extensional stiffness, to which the 10% rule directly applies, in the context of a material strength constraint, is not reflected in the design space for bending stiffness. This implies that the impact on buckling strength is not significant.

Table 2 demonstrate the number of laminate designs for *Extension-Shearing Bending-Twisting* coupled laminate designs with respect to ply contiguity constraints (1, ≤2 and ≤3) within the 10% rule design space. These results demonstrate that the common contiguity constraint of having no more than 3 adjacent plies with the same orientation, closely matches the constraint of the 10% rule across many of the ply number groupings with up to ($n$ =) 18 plies, for both symmetric and non-symmetric designs.

## 4 Conclusions

- New insights have been given for optimum compression and shear buckling strength for infinitely long plates, through the superposition of contour maps onto the lamination parameter design space for composite laminates with *Bending-Twisting* coupling.
- The impact of the 10% rule has also been illustrated on the reduced lamination parameter design space for extensional stiffness, for both symmetric and non-symmetric designs, containing all solutions with standard ply orientations and up to 18 plies. By contrast, there is no visible impact on the extent of the design space for bending stiffness, which implies that buckling strength is not indirectly affected by the application of the 10% design rule.
- The reduced design space, resulting from the application of the 10% rule, has been shown to be virtually identical to the application of the common design constraint of limiting the number of contiguous plies, i.e. adjacent plies with the same orientation, to a maximum of 3.

## REFERENCES

[1] C. B. York and S. F. M. Almeida, On extension-shearing bending-twisting coupled laminates, *Composite Structures*, **164**, 2017, pp. 10-22 (doi: 10.1016/j.compstruct.2016.12.041).

[2] C. B. York, On bending-twisting coupled laminates, *Composite Structures*, **160**, 2017, pp. 887-900 (doi: 10.1016/j.compstruct.2016.10.063).

[3] J. A. Bailie, R. P. Ley, and A. Pasricha, *A summary and review of composite laminate design guidelines*, Task 22, NASA Contract NAS1-19347, 1997.

[4] S. W. Tsai and H. T. Hahn, *Introduction to composite materials*, Technomic Publishing Co. Inc., Lancaster, 1980.

[5] M. P. Nemeth, Importance of Anisotropy on Buckling of Compression-Loaded Symmetric Composite Plates, *AIAA Journal*, 24(11), 1986, pp. 1831-1835.

[6] M. P. Nemeth, Buckling of symmetrically laminated plates with compression, shear, and in-plane bending, *AIAA Journal*, 30(12), 1992, pp. 2959-2965.

[7] J. Loughlan, The shear buckling behaviour of thin composite plates with particular reference to the effects of bend-twist coupling, *International Journal of Mechanical Sciences*, 43, 2001, pp. 771-792.

[8] J. E. Herencia, P. M. Weaver and M. I. Friswell, Closed-form solutions for buckling of long anisotropic plates with various boundary conditions under axial compression. *Journal of Engineering Mechanics*, 136, 2010, pp. 1105-1114.

[9] A. Baucke, C. Mittelstedt, Closed-form analysis of the buckling loads of composite laminates under uniaxial compressive load explicitly accounting for bending–twisting-coupling. *Composite Structures*, 128, 2015, pp. 437-454.

[10] C. B. York, Characterization of non-symmetric forms of fully orthotropic laminates, *Journal of Aircraft*, **46**(4), 2009, pp. 1114-1125 (doi:10.2514/1.32938).

[11] F. W. Williams, D. Kennedy, R. Butler and M. S. Anderson, VICONOPT: Program for exact vibration and buckling analysis or design of prismatic plate assemblies. *AIAA J.* 29, 1991, pp. 1927-1928.

[12] R. V. Southwell and S. W. Skan, On the stability under shear forces of a flat elastic strip, *Proceedings of the Royal Society of London*, A105, 1924, pp. 582-607.

| | $\xi^D_{\Delta c}$ | | | | | | | | | |
|---|---|---|---|---|---|---|---|---|---|---|
| | 0 | .1 | .2 | .3 | .4 | .5 | .6 | .7 | .8 | .9 |
| $c_1$ | 4.000 | 3.976 | 3.903 | 3.781 | 3.606 | 3.374 | 3.078 | 2.708 | 2.198 | 1.903 |
| $c_2$ | 0.000 | -0.014 | -0.054 | -0.119 | -0.210 | -0.329 | -0.481 | -0.674 | -0.905 | -1.384 |
| $c_3$ | -1.049 | -1.049 | -1.049 | -1.050 | -1.053 | -1.060 | -1.078 | -1.099 | -1.369 | -0.042 |
| $c_4$ | -1.217 | -1.235 | -1.291 | -1.391 | -1.539 | -1.742 | -2.012 | -2.395 | -3.022 | -2.872 |
| $c_5$ | 0.000 | 0.000 | -0.001 | -0.003 | -0.006 | -0.012 | -0.024 | -0.008 | -0.421 | 2.058 |
| $c_6$ | 0.000 | 0.007 | 0.027 | 0.057 | 0.098 | 0.145 | 0.195 | 0.229 | 0.300 | -0.358 |
| $c_7$ | 0.000 | -0.014 | -0.073 | -0.185 | -0.360 | -0.598 | -0.894 | -1.195 | -1.324 | -1.151 |
| $c_8$ | 0.000 | -0.001 | 0.000 | -0.001 | -0.001 | -0.001 | -0.004 | 0.029 | -0.299 | 1.621 |
| $c_9$ | 0.000 | 0.004 | 0.009 | 0.009 | 0.003 | -0.014 | -0.044 | -0.108 | -0.114 | -1.027 |
| $c_{10}$ | 0.340 | 0.351 | 0.390 | 0.452 | 0.542 | 0.671 | 0.843 | 0.997 | 0.975 | 3.589 |
| $c_{11}$ | -0.360 | -0.399 | -0.509 | -0.697 | -0.993 | -1.456 | -2.213 | -3.501 | -5.882 | -11.944 |
| $c_{12}$ | 0.000 | 0.000 | 0.000 | 0.000 | 0.000 | 0.000 | -0.001 | 0.012 | -0.092 | 0.451 |
| $c_{13}$ | 0.000 | -0.002 | -0.003 | -0.004 | -0.004 | -0.003 | 0.001 | 0.003 | 0.055 | -0.238 |
| $c_{14}$ | -0.034 | -0.032 | -0.041 | -0.052 | -0.066 | -0.083 | -0.127 | -0.262 | -0.581 | 0.594 |
| $c_{15}$ | 0.000 | -0.018 | -0.047 | -0.068 | -0.065 | -0.008 | 0.159 | 0.561 | 1.484 | 3.064 |

Table 1 – Compression buckling coefficients for Eq. (2) for $0 \leq \xi^D_{\Delta c} < 1.0$.

| | (a) Symmetric laminates | | | | (b) Non-symmetric laminates | | | |
|---|---|---|---|---|---|---|---|---|
| *n* | 1 | ≤2 | ≤3 | 10% | 1 | ≤2 | ≤3 | 10% |
| 7 | 2 | | | 2 | | | | |
| 8 | | | | | | | | |
| 9 | 26 | 40 | 42 | 42 | 4 | 8 | | 8 |
| 10 | | 34 | | 36 | | | | |
| 11 | 94 | 150 | 190 | 192 | 8 | 38 | 48 | 48 |
| 12 | | 214 | 224 | 260 | 8 | 32 | 36 | 36 |
| 13 | 382 | 934 | 1,258 | 1,300 | 146 | 916 | 1,240 | 1,292 |
| 14 | | 1,114 | 1,264 | 1,560 | 36 | 412 | 560 | 592 |
| 15 | 1,380 | 4,796 | 6,940 | 7,320 | 924 | 14,212 | 19,970 | 21,152 |
| 16 | | 5,104 | 6,102 | 7,882 | 266 | 5,554 | 8,498 | 9,288 |
| 17 | 4,720 | 21,840 | 33,478 | 36,176 | 6,582 | 165,022 | 251,098 | 270,848 |
| 18 | | 22,016 | 27,772 | 37,212 | 1,896 | 62,632 | 102,178 | 114,638 |

Table 2 – Effect of contiguity constraint and 10% design rule for: (a) Symmetric and; (b) Non-symmetric (Angle- and Cross-ply) *Extension-Shearing Bending-Twisting* coupled laminates.

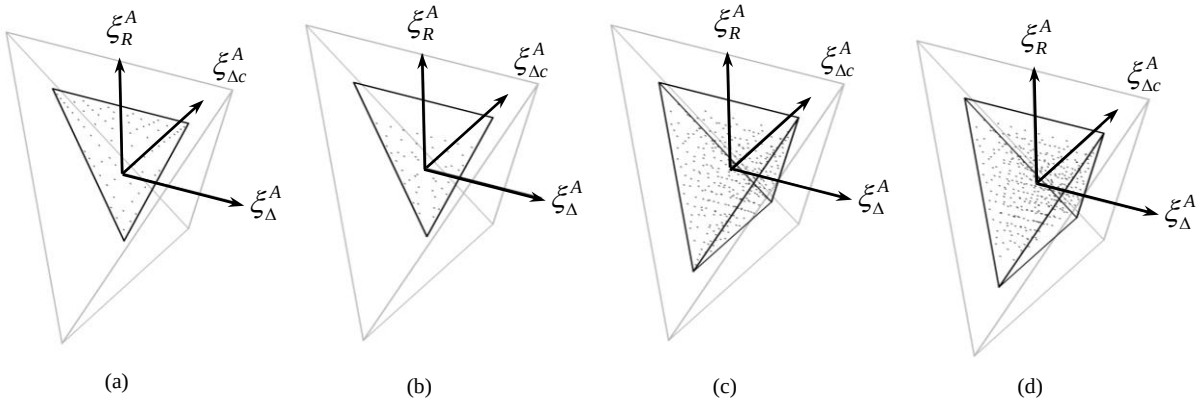


(a) (b) (c) (d)

Figure 1: Three dimensional lamination parameter design spaces for extensional stiffness, corresponding to: (a) Symmetric and (b) Non-symmetric *Bending-Twisting* coupled laminates with up to 18 plies and; (c) Symmetric and (d) Non-symmetric *Extension-Shearing Bending-Twisting* coupled laminates with up to 18 plies.

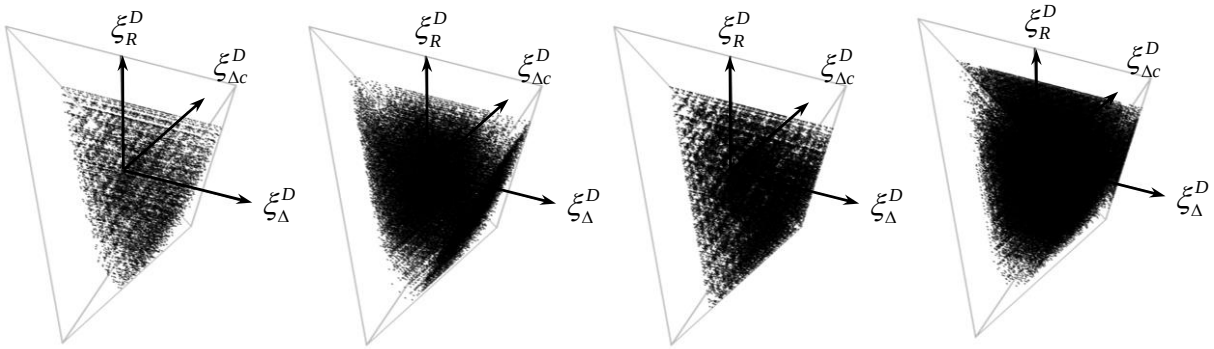


(a) (b) (c) (d)

Figure 2: Three dimensional lamination parameter design spaces for bending stiffness, corresponding to: (a) Symmetric and (b) Non-symmetric *Bending-Twisting* coupled laminates with up to 18 plies and; (c) Symmetric and (d) Non-symmetric *Extension-Shearing Bending-Twisting* coupled laminates with up to 18 plies.

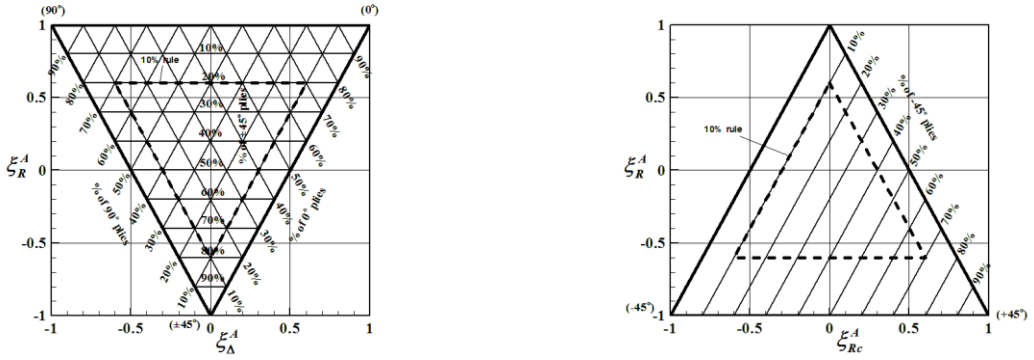


(a) (b)

Figure 3: Lamination parameter design space with ply percentage mapping for: (a) orthotropic stiffness ( $\xi_\Delta^A$ , $\xi_R^A$ ) and; (b) anisotropic stiffness ( $\xi_{\Delta c}^A$ ) relating to differing angle-ply percentages. The 10% design rule constraint is also illustrated.

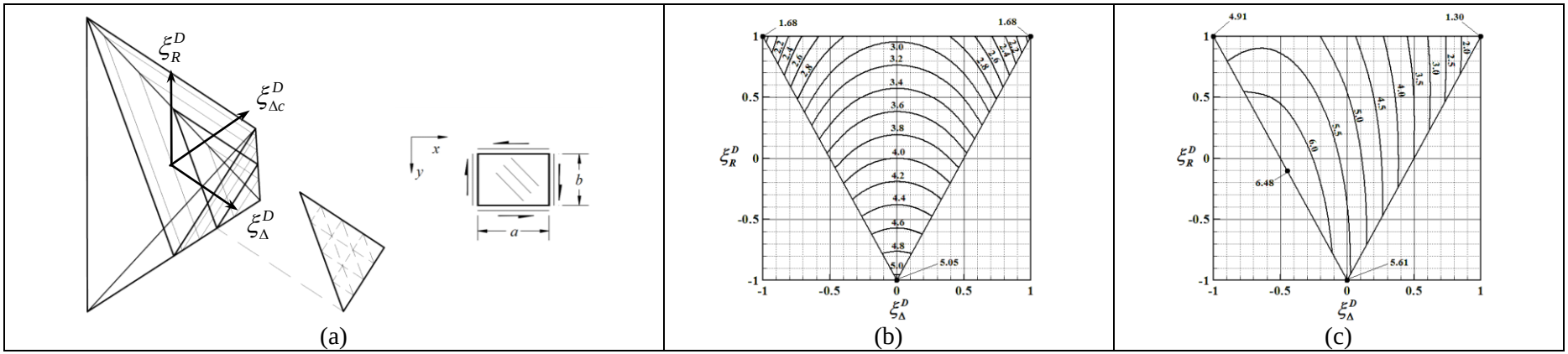


Figure 4: Three-dimensional representation of the feasible design space indicating (a) the positions through which two dimensional cross-sections have been taken. Positive shear load and positive fibre orientation are defined in the thumbnail sketch. Sections representing fully uncoupled laminates [10] in bending, correspond to: (b) compression buckling contours, $k_{x,\infty}$ (= $N_x b^2/\pi^2 D_{Iso}$) and; (c) positive/negative shear buckling contours, $k_{xy,\infty}$ (= $N_{xy} b^2/\pi^2 D_{Iso}$).

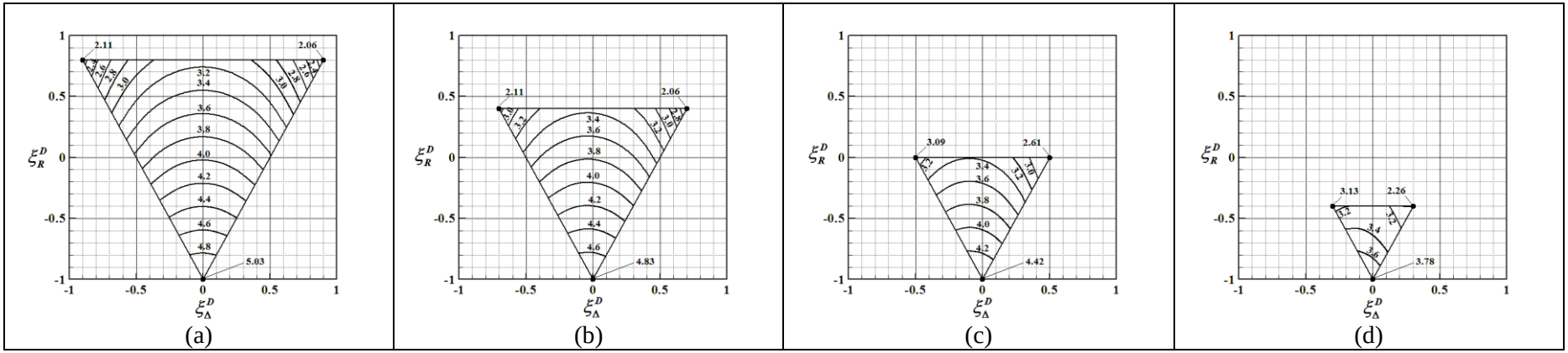


Figure 5: Compression buckling factor contours, $k_{x,\infty}$ (= $N_{xy} b^2/\pi^2 D_{Iso}$), for: (a) $\xi_{\Delta c}^D$ = 0.1: $\xi_{\Delta c}^D$ = 0.3, $\xi_{\Delta c}^D$ = 0.5 and $\xi_{\Delta c}^D$ = 0.7, representing *Bending-Twisting* coupled laminates.

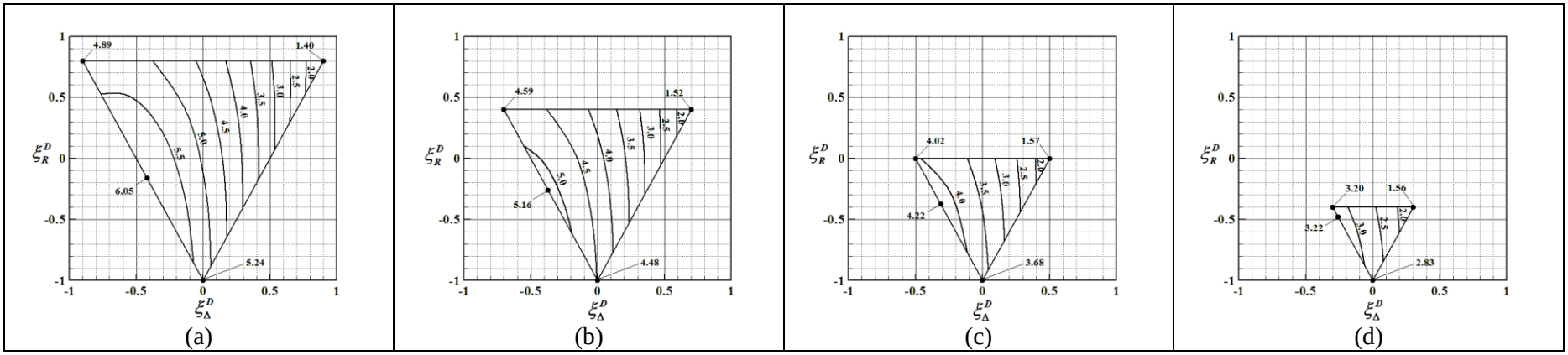


Figure 6 – Positive shear buckling factor contours, $k_{xy,\infty}$ (= $N_{xy}b^2/\pi^2 D_{Iso}$), for: (a) $\xi^D_{\Delta c}$ = 0.1: $\xi^D_{\Delta c}$ = 0.3, $\xi^D_{\Delta c}$ = 0.5 and $\xi^D_{\Delta c}$ = 0.7, representing *Bending-Twisting* coupled laminates.

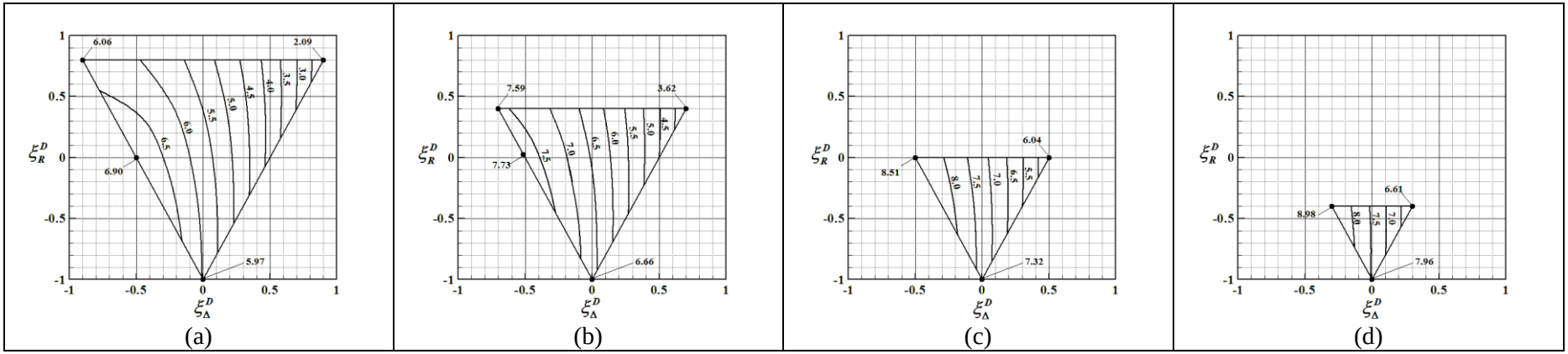


Figure 7 – Negative shear buckling factor contours, $k_{xy,\infty}$ (= $N_{xy}b^2/\pi^2 D_{Iso}$), for: (a) $\xi^D_{\Delta c}$ = 0.1: $\xi^D_{\Delta c}$ = 0.3, $\xi^D_{\Delta c}$ = 0.5 and $\xi^D_{\Delta c}$ = 0.7, representing *Bending-Twisting* coupled laminates.

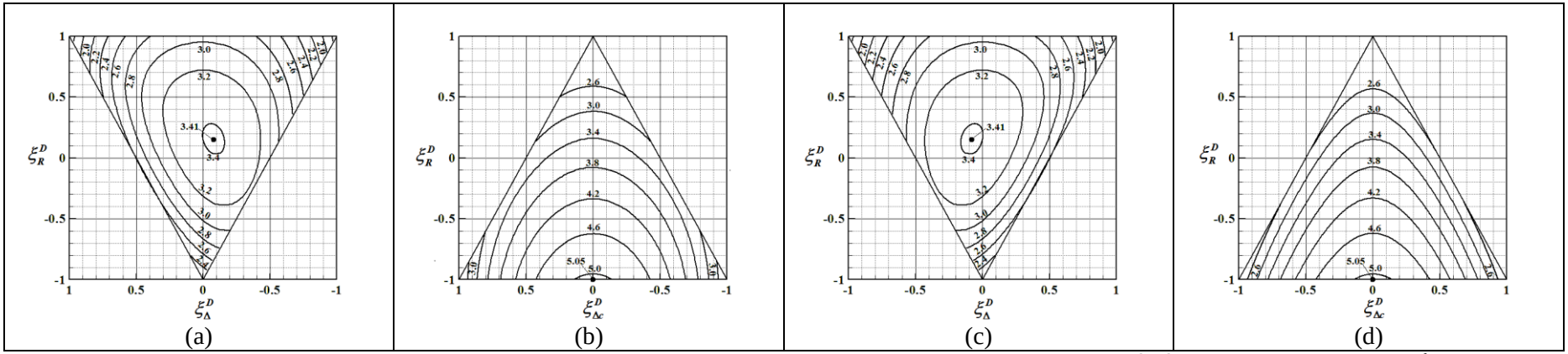


Figure 8: Lamination parameter design space surface contours for Compression buckling factor, $k_{x,\infty}$ (= $N_x b^2/\pi^2 D_{Iso}$), corresponding to 3rd angle orthographic projections of: (a) Rear (sloping) face with; (b) Left (sloping) face; (c) Front (sloping) face and; Right (sloping) face.

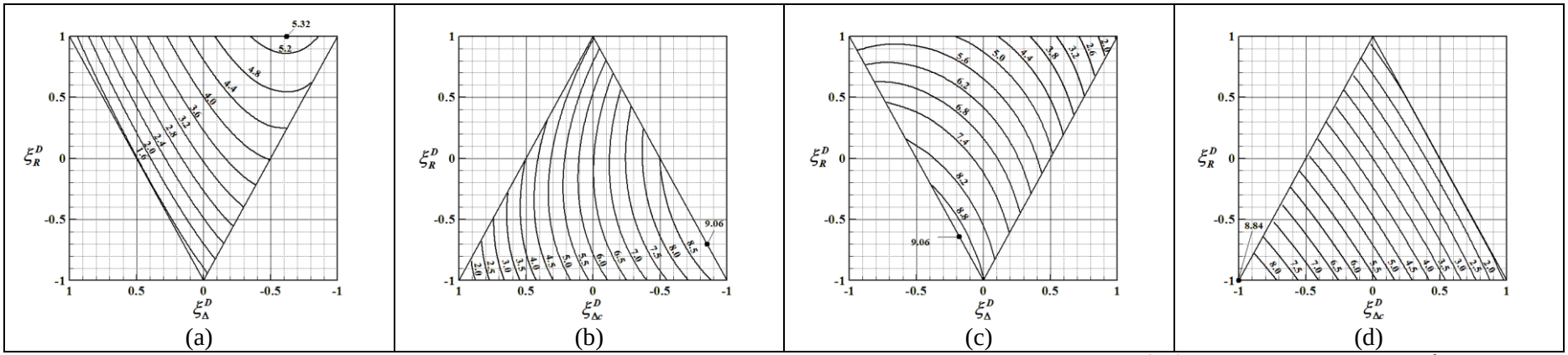


Figure 9: Lamination parameter design space surface contours for Positive Shear buckling factor, $k_{xy,\infty}$ (= $N_x b^2/\pi^2 D_{Iso}$), corresponding to 3rd angle orthographic projections of: (a) Rear (sloping) face; (b) Left (sloping) face; (c) Front (sloping) face and; Right (sloping) face.

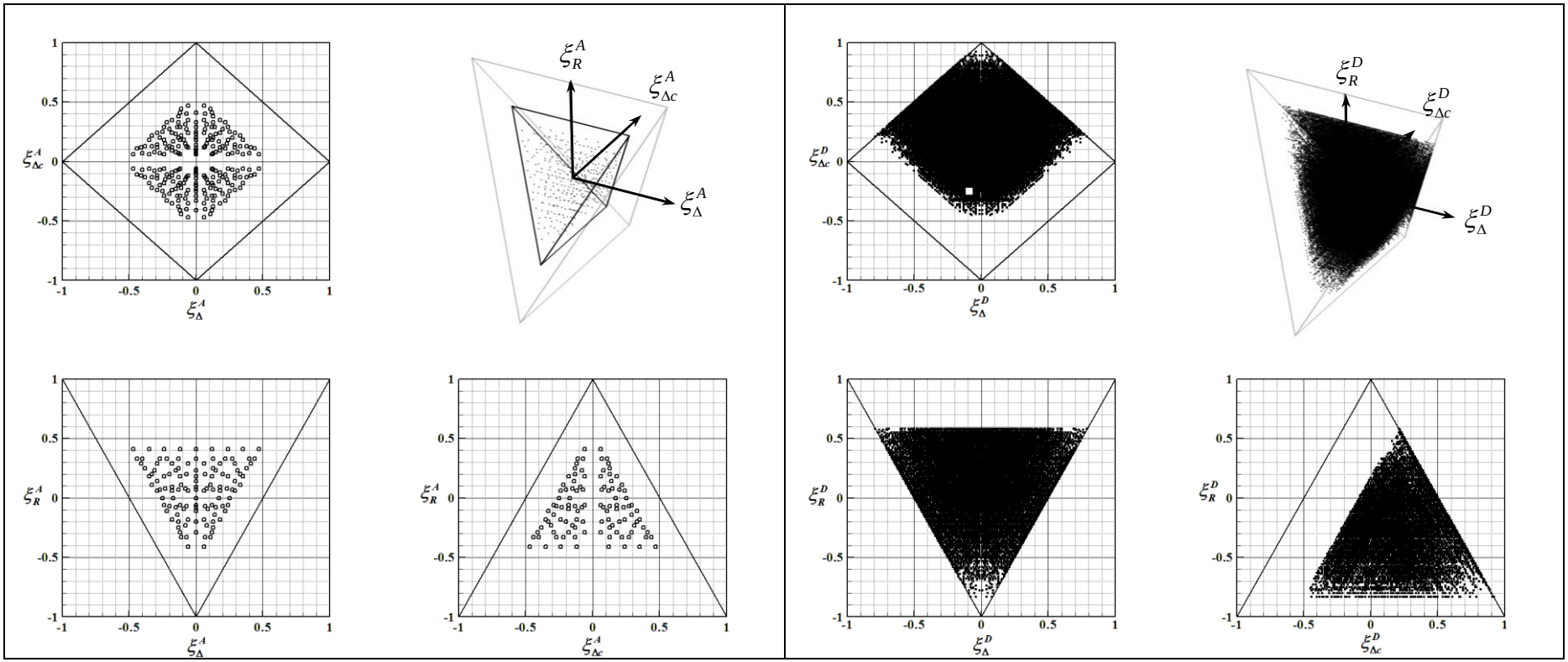


Figure 10 – Lamination parameter design spaces for non-symmetric *Extension-Shearing Bending-Twisting* coupled laminates with $7 \leq n \leq 18$, corresponding to orthographic projections (plan, front elevation and side elevation) for extensional ( $\xi_{\Delta}^{A}$ , $\xi_{R}^{A}$ , $\xi_{\Delta c}^{A}$ ) and bending stiffness ( $\xi_{\Delta}^{D}$ , $\xi_{R}^{D}$ , $\xi_{\Delta c}^{D}$ ).

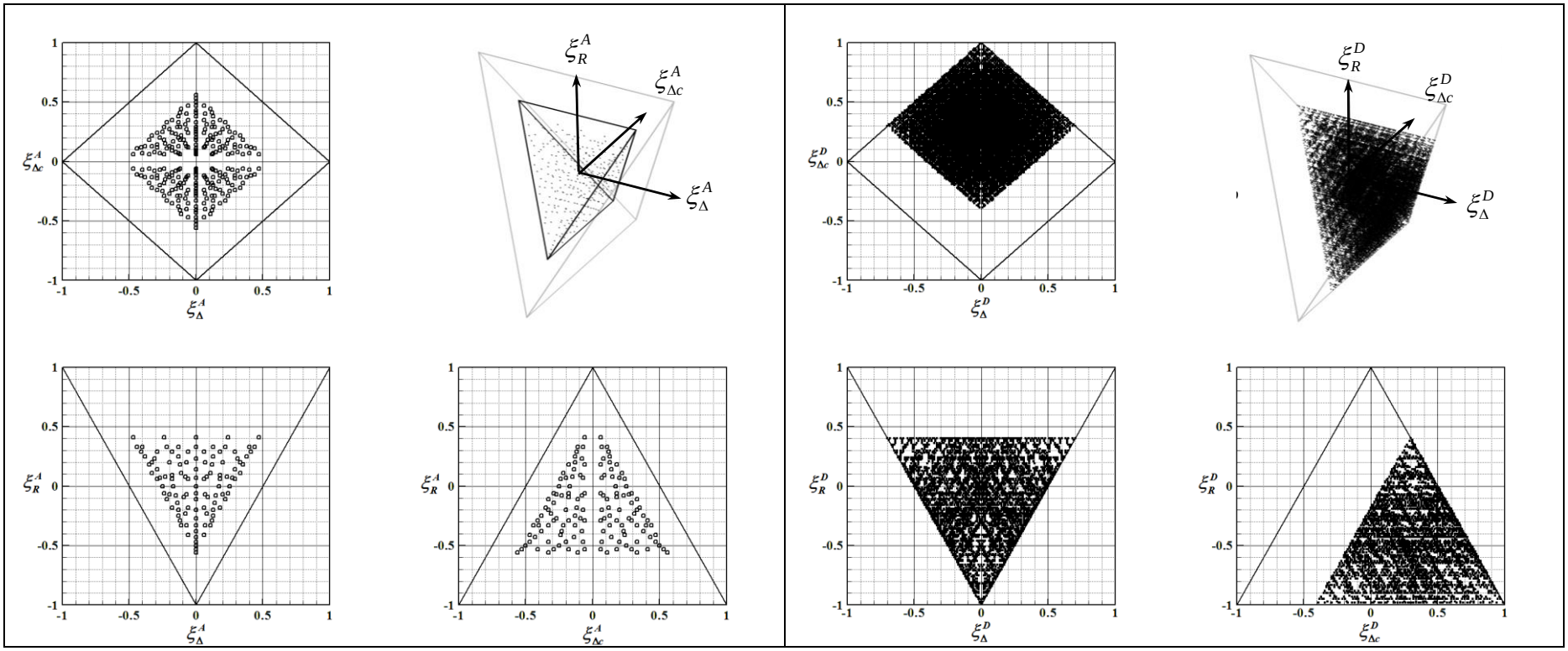


Figure 11 – Lamination parameter design spaces for symmetric *Extension-Shearing Bending-Twisting* coupled laminates with $7 \leq n \leq 18$, corresponding to orthographic projections (plan, front elevation and side elevation) for extensional ( $\xi^A_{\Delta}$ , $\xi^A_R$ , $\xi^A_{\Delta c}$ ) and bending stiffness ( $\xi^D_{\Delta}$ , $\xi^D_R$ , $\xi^D_{\Delta c}$ ).